




## RESEARCH

# Perforated ZnO nanoflakes as a new feature of ZnO achieved by the hydrothermal-assisted sol–gel technique

Zahra Khaghanpour<sup>1</sup> · Sanaz Naghibi<sup>1</sup> Received: 21 November 2016 / Accepted: 4 January 2017 / Published online: 23 January 2017  
© The Author(s) 2017. This article is published with open access at [Springerlink.com](http://Springerlink.com)

**Abstract** The perforated ZnO nanoflakes with high degree of crystallinity and uniformity were synthesized via the hydrothermal-assisted sol–gel technique without any template. ZnCl<sub>2</sub> was used as a Zn-containing precursor, causing the oriented growth of particles. The observation of a hole on the facet of the as-synthesized particles was discussed in this work. XRD, TEM, and DRS were used to investigate the prepared powder and a simple mechanism was suggested to explain the hole formation on the surface of nanoflakes. As a result, the synthesized powder included pure ZnO with direct band gap energy of 3.24 eV. The range of particle size was within 1 μm in diameter and <50 nm in thickness. A circle hole with 300–500 nm in diameter was observed on the facet of the as-synthesized particles.

**Keywords** ZnO nanoflakes · Perforated flake · Hydrothermal · ZnCl<sub>2</sub> · TEM

## Introduction

The hollow and perforated particles have recently attracted several scientists. For this reason, several methods and techniques have been presented and the improvement of the properties and the characteristics of the particles have been identified. Due to the unique morphology, the perforated particles have found specific applications in bio-science, energy storage, conversion, and adsorbents [1–4].

ZnO as a well-known ceramic material has become an interesting topic for several researches, and numerous preparation routs [5, 6], morphologies [7–10], and characteristics [11, 12] have been reported. The crystal structure of ZnO wurtzite is hexagonal. Zn and O atoms fill the crystallographic planes and form their unit cell. The anisotropic growth of ZnO crystallites is related to this structure, forming a large variety of features [13]. Morphology control of ZnO particles is an important parameter determining structure characteristics. Varieties of morphologies of ZnO particles have been synthesized with rod-like, hexagonal pyramid-like, truncated hexagonal conical, cauliflower-like, tubular, hourglass-like, flake-like, aggregate, and spherical shapes [7–10].

Nguyen et al. have been developed a template-based method for the preparation of hollow particles. In this approach, the ZnO hollow particles were synthesized via facilitating nucleation of ZnO crystallites under ultrasonic treatment. This process caused rising pressure and temperature at the interface between the cavitation bubbles (generated by ultrasonic vibrations) and the precursor solution. The solution temperature was measured up to 150 °C. In such circumstances, sol–gel stages (i.e., hydrolysis, pyrolysis, and condensation) occurred around the bubbles. In other word, the cavitation bubbles played important role in this process by providing uniform templates for the formation of hollow ZnO structure [14].

Zhang et al. have been synthesized ZnO hollow spheres by utilizing carbon microspheres as templates. In this process, Zn precursor was dissolved in dimethylformamide (DMF). Carbon microspheres as the sacrificial template and water as the hydrolysis agent were added to the solution. After a while, a puce precipitate was obtained. ZnO hollow spheres were obtained by heat treating the precipitated powder at 450 °C [15].

✉ Sanaz Naghibi  
naghibi@iaush.ac.ir

<sup>1</sup> Department of Materials Engineering, Shahreza Branch, Islamic Azad University, Pasdaran St., PO Box 86145-311, Shahreza, Isfahan Province, Iran

Jin et al. have been prepared hollow ZnO microsphere by a chemical method using polymethyl methacrylate (PMMA) as template. For this reason, PMMA powder, distilled water, and ammonia were mixed. After a while, Zn precursor was added to the solution, and then, the pH was adjusted to 8.5 using NaOH. The obtained precipitated powder was calcined at 350 °C. The synthesized microspheres were comprised of several layers of ZnO particles with hollow diameter of  $\sim 10 \mu\text{m}$ . [16].

Zhu et al. have used electrospinning and subsequent heat treatment to achieve hollow ZnO nanospheres. For this reason, Zn precursor was dissolved in distilled water and then added to the solution of polyvinyl pyrrolidone and ethanol. The obtained solution was applied by electrospinning process. The hollow ZnO nanospheres with an average diameter of  $\sim 250 \text{ nm}$  were formed [17].

As can be seen, most of the researches have been focusing on using sacrificial template to achieve the hollow structures.

This paper focused on introducing a new morphology of ZnO particles. The hydrothermal-assisted sol–gel method was applied and zinc chloride was used as the Zn precursor. As a result, 2D ZnO hexagonal single crystals with dimension of  $>1 \mu\text{m}$  were obtained. Interestingly, there are micron-sized hole on the as-synthesized ZnO flaks. It should be mentioned that this procedure is a template-less method. This phenomenon and its plausible mechanism will be explained.

## Materials and methods

In this work, zinc chloride ( $\text{ZnCl}_2$ , 99.8%, Merck, Germany), triethylamine (TEA,  $>99\%$ , Merck), and distilled water were used as the precursor, pH adjusting reagent, and solvent, respectively. An adequate amount of  $\text{ZnCl}_2$  was added to water to achieve a clear solution with the concentration of 5 g/L. Then, TEA was added to the stirring solution to make the pH reach 9. The precipitation occurred after 24 h and a white suspension achieved. This suspension was then treated by an autoclave for 2 h at 200 °C, and dried in an oven to obtain a white powder.

This powder sample was characterized using X-ray diffraction analysis, XRD (by a PANalytical's diffractometers, X'Pert Pro., The Netherlands), transmission electron microscopy, TEM (by a LEO equipment, Japan), as well as diffuse reflection spectroscopy, DRS (by a UV–visible scanning spectrophotometer, JASCO, Japan).

Based on the DRS results, the direct bandgap energy ( $E_g$ ) was measured in accordance with the Tauc method explained elsewhere [18], via plotting  $(\alpha h\nu)^2$  versus  $h\nu$ , where  $\alpha$  and  $h\nu$  are the photon energy and the absorption coefficient, respectively. The linear part of the curve extrapolated to  $h\nu$  axis to achieve  $E_g$  value.

The photocatalytic behaviors of the synthesized sample as well as  $\text{TiO}_2\text{-P25}$  were investigated via measuring the degradation of methylene blue as described previously [19]. For this reason, 100 mg of the powder samples were added to the methylene blue solution (30 mg/L), continuously stirred. The obtained suspensions were irradiated under UV lamp. The decomposition of methylene blue versus irradiation time was recorded by a UV–visible spectrophotometer. For this purpose, variation of the concentration, which is expressed as  $\ln C_0/C$  (where  $C_0$  refers to the initial concentration of methylene blue solution and  $C$  depicts the concentration of methylene blue after UV irradiation), was plotted versus time of UV exposure (30, 60, 90, and 120 min).

$\text{TiO}_2\text{-P25}$  (Degussa, Germany) is one of the well-known commercial semiconductors. Expression characteristics of this powder along with the obtained results (about the as-synthesized ZnO sample) could be useful for readers to give more detail on the interpretation of the characterizations.

## Results and discussion

Figure 1 shows the XRD pattern of the sample, which can be attributed to the wurtzite [JCPDS: 75–576] with a space group of  $P6_3mc$  and hexagonal crystal system without any

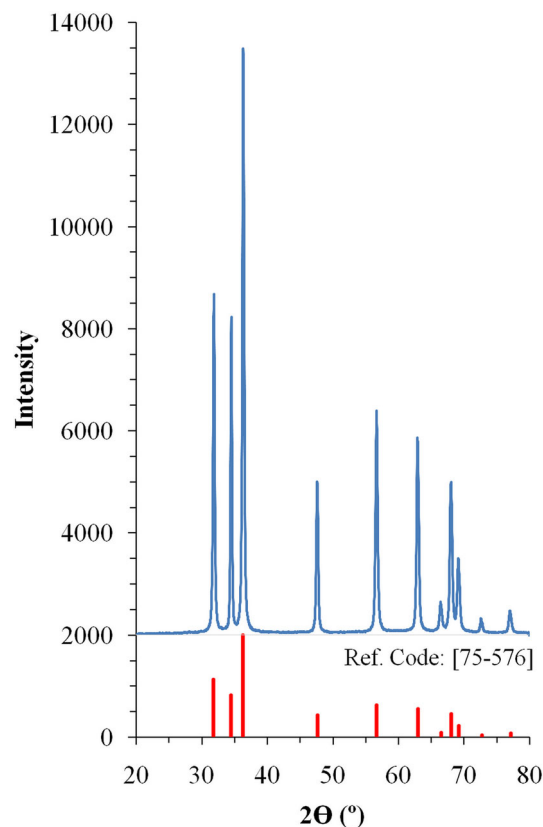


**Fig. 1** XRD pattern of the as-synthesized powder along with the peaks of ZnO [JCPDS: 75–576]

**Table 1** Experimentally acquired peaks position and intensity along with the standard parameters of ZnO [JCPDS: 75–576]

Peak no.	Observed position [ $^{\circ}2\Theta$ ]	Standard position [ $^{\circ}2\Theta$ ]	Observed intensity [cts, (%*)]	Standard intensity [cts]	Intensity changes** [%]	Observed d-spacing [Å]	Standard d-spacing [Å]	d-spacing changes*** [%]	Miller index
1	31.88	31.840	6395 (57)	56.1	+2	2.80,635	2.80,826	−0.07	100
2	34.53	34.503	5818 (52)	41.2	+26	2.59,717	2.59,740	−0.01	002
3	36.37	36.337	11,133 (100)	99.9	0	2.46,968	2.47,039	−0.03	101
4	47.65	47.653	2861 (26)	21.5	+21	1.9085	1.90,683	0.09	102
5	56.70	56.731	4192 (38)	30.9	+23	1.62,345	1.62,135	0.13	110
6	62.89	63.016	3492 (31)	27.2	+14	1.47,638	1.47,393	0.17	103
7	66.46	66.541	506 (5)	41.0	−88	1.40,562	1.40,413	0.11	200
8	67.98	68.120	2734 (25)	22.7	+10	1.37,779	1.37,538	0.18	112
9	69.20	69.261	1318 (12)	11.2	+7	1.35,648	1.35,549	0.07	201
10	72.59	72.759	258 (2)	18.0	−89	1.30,123	1.29,870	0.19	004
11	76.99	77.162	402 (4)	35.0	−89	1.23,751	1.23,520	0.19	202

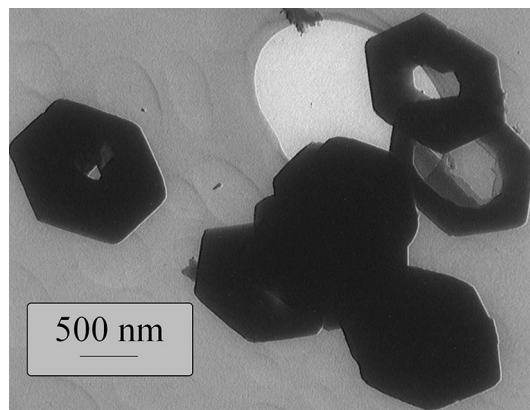
\* The observed height = (peaks height/11,133)  $\times$  100; These values can be compared to the standard intensities

\*\* Intensity changes = [(Observed Intensity-Standard Intensity)/Standard Intensity]  $\times$  100

\*\*\* d-spacing changes = [(Observed d-spacing-Standard d-spacing)/Standard d-spacing]  $\times$  100

impurity. Table 1 presents all the experimentally acquired peaks position and intensity along with the standard parameters of this phase. The comparison between the intensity and d-spacing values of the standard ZnO as well as the observed pattern indicated that the as-synthesized particles may not be formed in regular shape. The orientated growth may occur in this process. By considering the intensity of the highest observed peak at  $2\Theta = 36.37^{\circ}$  as 100%, the relative intensities of the other peaks show that there are changes in some of the diffraction angles, such as  $34.53^{\circ}$ ,  $56.70^{\circ}$ ,  $66.46^{\circ}$ ,  $72.59^{\circ}$ , and  $76.99^{\circ}$ . On the other hand, the interplanar spacing values show changes compared to the standard values in the orientation along  $\langle 10\bar{1}3 \rangle$ ,  $\langle 11\bar{2}2 \rangle$ ,  $\langle 0004 \rangle$ , and  $\langle 20\bar{2}2 \rangle$  directions. To evaluate this assertion, TEM could be useful equipment.

Figure 2 shows the TEM image of the as-synthesized powder. The hexagonal flake-like particles are observed with approximately  $\varnothing = 1 \mu\text{m}$  and oriented in  $\langle 0001 \rangle$  direction [20]. This feature is due to the inherent structure of wurtzite. In addition, the thickness of the particles was  $< 50 \text{ nm}$ ; therefore, these particles could be considered nanoflakes, which are similar to the other researchers' results [9, 20]. This irregularity is related to the crystal growth along  $c$  orientation. The ZnO crystallites are known as polar molecules, so that their polar faces are capable to absorb ions from the solution, in contrary ion adsorption along  $c$  axis are restricted, and then, the growth along this axis declines. This is the reason of the flaky particles formation. Since TEA acts as a catalyst in this system [21],  $\text{ZnCl}_2$  ionizes into  $\text{Zn}^{2+}$  and  $\text{Cl}^-$ . The  $\text{Zn}^{2+}$  participates in the crystallization

**Fig. 2** TEM image of the as-synthesized powder

reactions, whereas  $\text{Cl}^-$  ions determine the final feature of the particles. These ions adhere to the (0001) facet of the crystallites and hinder the proximity of  $\text{Zn}^{2+}$  and the crystallites surface [22].

The motivation for this work refers to the existence of a unique hole on the ZnO nanoflakes. This phenomenon has not been reported before, and this paper attempts to propose an impressive mechanism to investigate the preparation of perforated particles.

Figure 3 shows the schematic illustration of the suggested mechanism. In the early stages of the homogeneous nucleation,  $\text{Zn}(\text{OH})_2$  molecules have an important role. Increasing time and temperature of the hydrothermal vessel causes to provide the nucleation condition. When the initial ZnO crystallites appear in the solution (Fig. 3I),  $\text{Zn}^{2+}$  ions congregate around them (Fig. 3II). The  $\text{Cl}^-$  ions surround  $\text{Zn}^{2+}$  ions; therefore,  $\text{Zn}^{2+}$  ions

**Fig. 3** Schematic illustration of the mechanism of the formation of holes

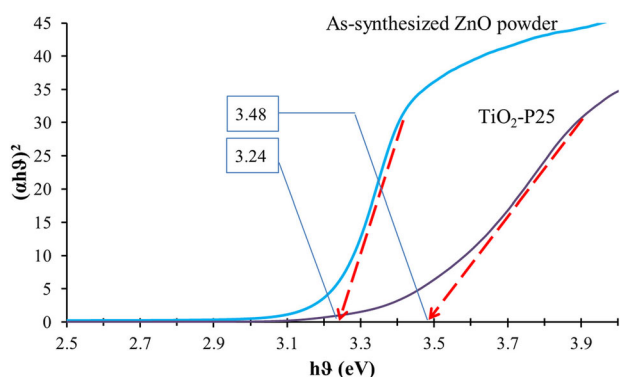
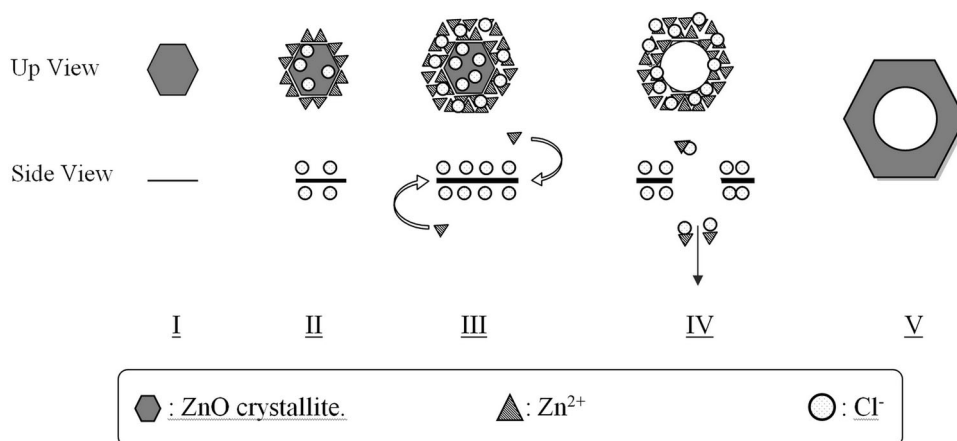


**Fig. 4** Tauc results for ZnO powder

congregate on the edges and addition of the  $\text{Zn}^{2+}$  ions onto the facet become restricted (Fig. 3III). The conversion of intermediate product to the oxide form needs sufficient time and energy. In this period,  $\text{Cl}^-$  ions, which are accumulated close to the center of the crystallite, would probably participate in reaction to  $\text{Zn}^{2+}$  ions and remove them from the gathering place. This can led to form a hole through a particle (Fig. 3IV). This irregular feature could be considered the reason of the changes in the XRD results, which was previously explained (see Table 1).

As ZnO powder is known as a photocatalyst, the optical behavior of the as-synthesized powder should be studied.

Figure 4 represents the optical characteristics of the ZnO nanoflakes and  $\text{TiO}_2$ -P25 powder, providing  $E_g$  of nanoflakes and P25 as 3.24 and 3.48 eV, respectively. The  $E_g$  value of ZnO powder has been reported in the range of 3.26–3.30 eV [23–25]. This approved that the mentioned morphology cannot essentially affect  $E_g$ .

Figure 5 shows the kinetics of the photocatalytic degradation of methylene blue suspension containing the as-synthesized ZnO and  $\text{TiO}_2$ -P25 powders. By accordance with the  $\ln(C_0/C)$  versus irradiation time, the first-order kinetic model is valid for both samples, but the

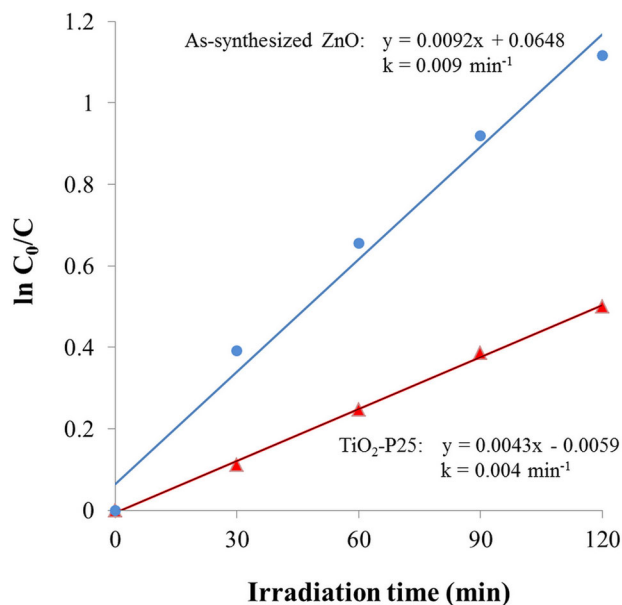


**Fig. 5** Kinetics model of the photodegradation of dye solution containing as-synthesized ZnO powder (filled circles), and  $\text{TiO}_2$ -P25 powder (filled triangle)

lines slope show higher photoactivity of the as-synthesized powder in comparison with  $\text{TiO}_2$ -P25 nanoparticles. In other words,  $k_{\text{ZnO}}$  ( $0.009 \text{ min}^{-1}$ ) is more than  $k_{\text{P25}}$  ( $0.004 \text{ min}^{-1}$ ). Despite the smaller particle size of P25 and relatively similar band gap energy, as-synthesized ZnO powder indicates lower photoactivity. This characteristic is correlated to the higher specific surface area, larger pore volume, and higher degree of crystallinity [18]. The observed phenomenon can be referred to the higher surface area and lower  $E_g$  value of the as-synthesized powder.  $k_{\text{ZnO}}$  is more than two times greater than  $k_{\text{P25}}$ , whereas ZnO particle size is about  $1 \mu\text{m}$ ; 40 times greater than that of  $\text{TiO}_2$ -P25 (average particle size is about 25 nm). It may be related to the existence of the holes on the facet of ZnO particles.

## Conclusions

Perforated ZnO nanoflakes were fabricated using the hydrothermal-assisted sol-gel technique without any template. TEA, water, and ZnCl<sub>2</sub> were used as catalyst, solvent, and Zn precursor, respectively. Cl<sup>-</sup> ion was responsible for the oriented growth and the hole formation during the nucleation and growth of ZnO particles. They surrounded the crystallites of ZnO and prevented the addition of Zn<sup>2+</sup> to the surface. On the other hand, they probably participate in reaction to Zn<sup>2+</sup> and removed them from the vicinity of the crystallite, providing the condition for a hole formation. The synthesized powder consisted of ZnO wurtzite phase without any impurity and direct bandgap energy of 3.24 eV. The particles with 1 μm in diameter and less than 50 nm in thickness were observed. There were circle holes with 300–500 nm in diameter on the facet of the as-synthesized particles.

**Open Access** This article is distributed under the terms of the Creative Commons Attribution 4.0 International License (<http://creativecommons.org/licenses/by/4.0/>), which permits unrestricted use, distribution, and reproduction in any medium, provided you give appropriate credit to the original author(s) and the source, provide a link to the Creative Commons license, and indicate if changes were made.

## References

- Andreyev, D.S., Arriaga, E.A.: Fabrication of perforated sub-micron silica shells. *Scr. Mater.* **57**(10), 957–959 (2007)
- Chen, A., Li, Y., Yu, Y., Li, Y., Xia, K., Wang, Y., Li, S., Zhang, L.: Synthesis of hollow mesoporous carbon spheres via “dissolution-capture” method for effective phenol adsorption. *Carbon* **103**, 157–162 (2016)
- Zhao, T., Luo, W., Deng, Y., Luo, Y., Xu, P., Liu, Y., Wang, L., Ren, Y., Jiang, W.: Monodisperse mesoporous TiO<sub>2</sub> microspheres for dye sensitized solar cells. *Nano Energy* **26**, 16–25 (2016)
- Liu, J., Hui, A., Ma, J., Chen, Z., Peng, Y.: Fabrication and application of hollow ZnO nanospheres in antimicrobial casein-based coatings. *Int. J. Appl. Ceram. Technol.* (2016). doi:10.1111/ijac.12635
- Gharagozlou, M., Baradaran, Z., Bayati, R.: A green chemical method for synthesis of ZnO nanoparticles from solid-state decomposition of Schiff-bases derived from amino acid alanine complexes. *Ceram. Int.* **41**(7), 8382–8387 (2015)
- Gharagozlou, M., Naghibi, S.: Synthesis of ZnO nanoparticles based on Zn complex achieved from L-leucine. *J. Chin. Chem. Soc.* **63**(3), 290–297 (2016)
- Wang, H., Xie, J., Yan, K., Duan, M.: Growth mechanism of different morphologies of ZnO crystals prepared by hydrothermal method. *J. Mater. Sci. Technol.* **27**(2), 153–158 (2011)
- Xu, L., Hu, Y.-L., Pelligra, C., Chen, C.-H., Jin, L., Huang, H., Sithambaram, S., Aindow, M., Joesten, R., Suib, S.L.: ZnO with different morphologies synthesized by solvothermal methods for enhanced photocatalytic activity. *Chem. Mater.* **21**(13), 2875–2885 (2009)
- Li, H., Jiao, S., Li, H., Li, L.: Growth and characterization of ZnO nanoflakes by hydrothermal method: effect of hexamine concentration. *J. Mater. Sci. Mater. Electron.* **25**(6), 2569–2573 (2014)
- Liu, Y., Dong, J., Hesketh, P.J., Liu, M.: Synthesis and gas sensing properties of ZnO single crystal flakes. *J. Mater. Chem.* **15**(23), 2316–2320 (2005)
- Lee, C.-P., Chen, P.-W., Li, C.-T., Huang, Y.-J., Li, S.-R., Chang, L.-Y., Chen, P.-Y., Lin, L.-Y., Vittal, R., Sun, S.-S., Lin, J.-J., Ho, K.-C.: ZnO double layer film with a novel organic sensitizer as an efficient photoelectrode for dye-sensitized solar cells. *J. Power Sources* **325**, 209–219 (2016)
- Li, S.-Q., Zhou, P.-J., Zhang, W.-S., Chen, S., Peng, H.: Effective photocatalytic decolorization of methylene blue utilizing ZnO/rectorite nanocomposite under simulated solar irradiation. *J. Alloys Compd.* **616**, 227–234 (2014)
- Zinc oxide (ZnO) crystal structure, lattice parameters. In: Madelung, O., Rössler, U., Schulz, M. (eds.) II–VI and I–VII Compounds; Semimagnetic Compounds, pp. 1–5. Springer, Heidelberg (1999). Book DOI: 10.1007/b71137, Chapter DOI: 10.1007/10681719\_286
- Nguyen, D.T., Kim, K.-S.: Structural evolution of highly porous/hollow ZnO nanoparticles in sonochemical process. *Chem. Eng. J.* **276**, 11–19 (2015)
- Zhang, J., Wang, S., Wang, Y., Xu, M., Xia, H., Zhang, S., Huang, W., Guo, X., Wu, S.: ZnO hollow spheres: preparation, characterization, and gas sensing properties. *Sens. Actuators B Chem.* **139**(2), 411–417 (2009)
- Jin, D., Liao, N., Xu, X., Yu, X., Wang, L., Wang, L.: Synthesis of hollow ZnO microspheres and its novel UV absorption. *Mater. Chem. Phys.* **123**(2–3), 363–366 (2010)
- Zhu, C., Lu, B., Su, Q., Xie, E., Lan, W.: A simple method for the preparation of hollow ZnO nanospheres for use as a high performance photocatalyst. *Nanoscale* **4**(10), 3060–3064 (2012)
- Naghibi, S., Faghihi Sani, M.A., Madaah Hosseini, H.R.: Application of the statistical Taguchi method to optimize TiO<sub>2</sub> nanoparticles synthesis by the hydrothermal assisted sol-gel technique. *Ceram. Int.* **40**(3), 4193–4201 (2014)
- Naghibi, S., Madaah Hosseini, H.R., Faghihi Sani, M.A., Shokrgozar, M.A., Mehrjoo, M.: Mortality response of folate receptor-activated, PEG-functionalized TiO<sub>2</sub> nanoparticles for doxorubicin loading with and without ultraviolet irradiation. *Ceram. Int.* **40**(4), 5481–5488 (2014)
- Vabbina, P.K., Karabiyik, M., Al-Amin, C., Pala, N., Das, S., Choi, W., Saxena, T., Shur, M.: Controlled synthesis of single-crystalline ZnO nanoflakes on arbitrary substrates at ambient conditions. *Part. Part. Syst. Charact.* **31**(2), 190–194 (2014)
- Ghasemzadeh, M.A., Safaei-Ghomi, J., Weaver, G.: Synthesis and characterization of ZnO nanoparticles: application to one-pot synthesis of benzo[b][1,5]diazepines. *Cogent Chem.* **1**(1), 1095060 (2015)
- Sugunan, A., Warad, H.C., Boman, M., Dutta, J.: Zinc oxide nanowires in chemical bath on seeded substrates: role of hexamine. *J. Sol-Gel Sci. Technol.* **39**(1), 49–56 (2006)
- Meyer, B.K.: ZnO band structure, energy gaps. In: Rössler, U. (eds.) *New Data and Updates for IV–IV, III–V, II–VI and I–VII Compounds, their Mixed Crystals and Diluted Magnetic Semiconductors*, pp. 566–569. Springer, Heidelberg (2011). Book DOI: 10.1007/978-3-642-14148-5, Chapter DOI: 10.1007/978-3-642-14148-5\_316
- Deng, Z., Chen, M., Gu, G., Wu, L.: A facile method to fabricate ZnO hollow spheres and their photocatalytic property. *J. Phys. Chem. B* **112**(1), 16–22 (2008)
- Özgür, Ü., Alivov, Y.I., Liu, C., Teke, A., Reshchikov, M.A., Doğan, S., Avrutin, V., Cho, S.-J., Morkoç, H.: A comprehensive review of ZnO materials and devices. *J. Appl. Phys.* **98**(4), 041301 (2005). doi:10.1063/1.1992666

